Journal of Photochemistry & Photobiology A: Chemistry 364 (2018) 725–731

Contents lists available at ScienceDirect

Journal of Photochemistry & Photobiology A: Chemistry

journal homepage: www.elsevier.com/locate/jphotochem

Ultrastable photodegradation of formaldehyde under fluorescent lamp irradiation by anti-reflection structure SnS_2/TiO_2 composite

Guanhong Lu[a], Xiaofeng Xie[a,*], Xiao Wang[a], Gansheng Shi[a], Qinglong Zeng[a], Doris Segets[b], Jing Sun[a,*]

[a] Shanghai Institute of Ceramics, Chinese Academy of Sciences, 1295 Dingxi Road, Shanghai 200050, China
[b] Institute of Particle Technology (LFG), Interdisciplinary Center for Functional Particle Systems (FPS), Friedrich-Alexander-Universität Erlangen-Nürnberg (FAU), 91058 Erlangen, Germany

ARTICLE INFO

Keywords:
Photocatalysis
Formaldehyde
Anti-reflection
SnS_2
TiO_2

ABSTRACT

In this work, mesoporous titanium dioxide sphere Mp-TiO_2/SnS_2 composites have been synthesized for the photodegradation of formaldehyde with fluorescent lamp. SnS_2 nanosheets/nanoparticles were deposited on the surface of Mp-TiO_2 sphere uniformly through an in-situ method. The morphology of SnS_2 can be modulated through adjusting the Sn/Ti molar ratio. SnS_2 nanosheet turned into nanoparticle when the Sn/Ti molar ratio changed from 0.05 and 0.10 to 0.15 and 0.20. The physical and chemical properties of as-prepared composite catalysts were thoroughly studied by X-ray diffraction (XRD), Raman, scanning electron microscope (SEM), Brunauer Emmett Teller (BET), energy-dispersive X-ray spectroscopy (EDS), photoluminescence (PL) and UV–vis spectrophotometer. The photocatalytic performance of Mp-TiO_2/SnS_2 in the degradation of HCHO was assessed in a smog chamber with the irradiation of fluorescent light. A degradation efficiency of about 63% was achieved when the molar ratio of SnS_2/TiO_2 was 0.10. Through extending the light absorption range and hindering the recombination of photo-generated electron-hole pairs, the combination with SnS_2 enabled the fabrication of hybrid photocatalysts with high photocatalytic activity and long-term stability.

1. Introduction

Recently, air pollution has drawn a lot of attention due to its harm to human health. As one of the primary volatile organic compounds (VOCs) in indoor environment, formaldehyde (HCHO), which is emitted by the decoration materials and wooden furnishing materials, could cause nasal tumors, irritation of the eye mucosa, respiratory tract and skin irritation [1–7]. Photocatalysis technology, as an effective and low-cost 'green' method, provides a way to decompose air pollutants with low concentrations under light [8,9]. TiO_2 is one of the most promising materials for the photocatalytic decomposition of gaseous organic pollutants because of its high chemical stability, non-toxicity and low cost [10–14]. However, as an indirect bandgap semiconductor, the fast recombination of photo-generated electron–hole pairs in pure TiO_2 held back the generation of active radicals and the effective degradation of gaseous contaminants, which limited the application of TiO_2 in the field of indoor air purification [15–18].

Decorating the surface of TiO_2 nanoparticles with metal sulfide semiconductors has been regarded as an effective way for solving the above mentioned issues. The relative narrow band gap of sulfides enabled the utilization of visible light while the heterojunction formed on the interface between TiO_2 and sulfides promoted the separation of photon-generated charge carriers [19, 20]. Among them, CdS [21], $Zn_xCd_{1-x}S$ [22] and PbS [23] have been applied in the photocatalytic degradation of organic dyes and water splitting. However, the large-scale application of CdS and PbS were still limited due to their high toxicity. By contrast, SnS_2 has attracted a wide attention as a nontoxic, chemically stable, inexpensive and earth-abundant material, with a band gap within the range of 2.08–2.44 eV. Through a simple hydrothermal treatment, Zhang et al. deposited ultrathin hexagonal SnS_2 nanosheets on the electrospun TiO_2 nanofibers for the effective degradation of organic dyes (RhB and MO) and phenols (4-NP) [24]. Christoforidis et al. synthesized SnS_2 nanosheet-decorated TiO_2 anatase nanofibers for the highly-efficient degradation of gas-phase diethylsulfide [25]. However, to our best knowledge, no report is available on the potential application of TiO_2/SnS_2 compound materials in indoor air purification under the regular lower power indoor fluorescent lamp.

In addition, the factors that influence the photocatalytic reactions such as the morphology of TiO_2, have been widely researched [26–28]. Mesoporous titanium dioxide sphere (Mp-TiO_2) with a homogeneous

* Corresponding authors.
E-mail addresses: xxfshcn@163.com (X. Xie), jingsun@mail.sic.ac.cn (J. Sun).

https://doi.org/10.1016/j.jphotochem.2018.06.043
Received 31 March 2018; Received in revised form 11 June 2018; Accepted 27 June 2018
Available online 09 July 2018
1010-6030/

wormhole-like mesostructure has been synthesized in this work. The mesoporous structure with a large specific surface area is a considerable factor to provide more active sites via the means of boosting up the adsorption property. The multiple light reflections happened between the stacking spaces of TiO_2 spheres could further enhance its light harvesting efficiency. SnS_2 nanostructures were then in situ deposited on the Mp-TiO_2 through a hydrothermal process to get Mp-TiO_2/SnS_2 compounds. Herein, 2.5 ppm formaldehyde (HCHO) and two 20 w fluorescent lamps were used to simulate the indoor pollutant and indoor lighting sources, respectively. The highest photocatalytic degradation efficiency of 63% was achieved while applying Mp-TiO_2/SnS_2 compounds with the nominal Sn/Ti molar ratio of 0.10 as the photocatalyst. Furthermore, composite catalysts exerted an excellent photocatalytic stability in the indoor environment. These results greatly promoted the practical application of TiO_2-based photocatalytic materials in indoor air purification.

2. Experimental section

2.1. Preparation of mesoporous TiO_2 sphere powder

Mp-TiO_2 sphere with high specific surface area was prepared with a two-step method reported previously [29]. In a typical synthesis process, 7.95 g hexadecylamine (HDA) was dissolved in 800 ml anhydrous ethanol. 3.2 ml KCl solution (0.1 M) and 3.2 ml deionized water were then added to the solution. After the addition of 18 ml titanium(IV) isopropoxide (TIP), a milky white suspension was obtained under vigorous stirring. This suspension was aged for 16 h at room temperature and then filtered to separate the precipitate. The precipitate was then washed with ethanol for three times and dried in air at room temperature. 1.6 g as-prepared powder was treated through a solvothermal process at 160 °C for 16 h in the teflon-lined autoclave (50 ml) with the mixture of 20 ml ethanol, 10 ml deionized water and 0.5 ml 28% ammonia solution. Then, the mixed suspension was sealed within the reactor and aged at 160 °C for 16 h to make the TiO_2 powder crystallized. The resultant powders were calcined at 500 °C for 2 h in air to eliminate organic components and obtain mesoporous TiO_2.

2.2. Synthesis of Mp-TiO_2/SnS_2

Mp-TiO_2/SnS_2 was prepared by a hydrothermal method. Stannic chloride ($SnCl_4$) and thioacetamide (TAA) were dissolved in 50 ml deionized water. The Mp-TiO_2 powder was dispersed in the above solution and sonicated for 20 min. Then, the milky white suspension was sealed in a 100 mL teflon-lined autoclave and heated at 150 °C for 15 h. The resulting composite powder was washed by water and ethanol for several times and then calcined at 180 °C for 3 h in argon atmosphere (purity:99.999%). Herein, the Mp-TiO_2/SnS_2 composites with different Sn/Ti molar ratios of 0.05, 0.10, 0.15 and 0.20 (samples named as Sn (0.05)/Ti, Sn(0.10)/Ti, Sn(0.15)/Ti and Sn(0.20)/Ti, respectively) were synthesized with the above method. The weight of TiO_2 powder remained unchanged in all samples, while the concentration of $SnCl_4$ varied to achieve a nominal Sn/Ti molar ratio of 0.05, 0.10, 0.15 and 0.20. The molar ratio of $SnCl_4$ and TAA was kept constant at 0.5 in all samples. 0.1 g catalyst was coated on a 15 cm*7.5 cm glass substrate through the 'blade coating' method for the following evaluation of the photocatalytic activity.

2.3. Materials characterizations

The crystalline structure of the catalysts was measured by wide-angle X-ray diffractometer (XRD; Ultima IV 2036E102, Rigaku Corporation, Japan) using Cu Kα radiation at 50 Hz. The scan rate was 5°/min. Raman spectroscopy was carried out on the DXR Raman Microscope (ThermoFisher Scientific, USA). Photoluminescence spectra (PL) of samples were recorded using a fluorescent spectroscope (F-4600, Hitachi, Japan). The morphology and microstructure of the as-prepared Mp-TiO_2/SnS_2 was characterized by scanning electron microscope (SEM, SU8220, Hitachi, Japan). The adsorption properties of catalysts were measured by Brunauer, Emmett, and Teller (BET) nitrogen sorption surface area measurements, using an analyzer (Micromeritics ASAP 3000 system, Micromeritics, USA). The samples were degassed at 80 °C for 6 h below 26.7 Pa before the measurements. The optical properties of Mp-TiO_2/SnS_2 films were investigated by a UV–vis spectrophotometer (Lambda 950 UV/Vis spectrometer, Perkin Elmer, USA). Elemental analysis of the catalysts was carried out by an Energy Dispersive Spectrometer (EDS) (JXA-8100, JEOL, Japan).

2.4. Evaluation of photocatalytic activity

The catalytic activities of Mp-TiO_2/SnS_2 films were monitored by the degradation of formaldehyde (HCHO) under visible light (2*20 w fluorescent lamps purchased from Philips). The catalysts were illuminated by two 20 w fluorescent lamps vertically, and the distance between the catalyst and lamps was 15 cm. The concentration of HCHO was tested by 500 Series Intelligent Gas Detector (purchased from AeroQual Company) at room temperature. The relative humidity was controlled at 50% ± 5% in the whole photocatalytic process. The photocatalytic experiment was carried out as follows: (1) A clean plastic bag used as smog chamber was first sealed and vacuumed after putting the gas detector and catalyst inside; (2) Formaldehyde and clean air were added into the bag and then the operating system was kept in the dark for 20 min to make the mixed gas reaching a stable state; (3) The photocatalytic reaction was carried out under visible light irradiation. The photocatalytic degradation rate of HCHO was denoted as C/C_0, where C is the HCHO concentration at a given time, and C_0 is the initial concentration of HCHO. The volume of the smog chamber is 40 L.

3. Results and discussion

The XRD patterns of pure Mp-TiO_2 and Mp-TiO_2/SnS_2 powders with different Sn/Ti ratios are exhibited in Fig. 1. The main diffraction peaks at 25.28°, 37.80°, 48.05°, 53.89°, 55.06° and 62.69° could be assigned to the (101), (004), (200), (105), (211) and (204) crystal facets of anatase TiO_2 (PDF#21-1272), respectively. The diffraction peaks of as-deposited SnS_2 at 2θ = 15.03°, 28.20° and 49.96° could be indexed to the (001), (100) and (110) crystal faces of berndtite-2 T SnS_2 (PDF#23-0677), respectively. Moreover, the peaks of Mp-TiO_2 in the XRD pattern of Mp-TiO_2/SnS_2 composite powders with different molar ratio of Sn/Ti did not differ from pure Mp-TiO_2 powder, which demonstrated that the crystal structure of Mp-TiO_2 remained stable during the in-situ

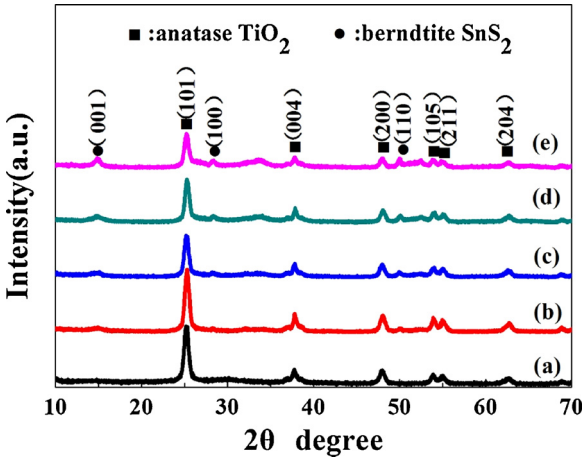

Fig. 1. XRD patterns of pure Mp-TiO_2 and Mp-TiO_2/SnS_2 composite films with the different ratios of Sn/Ti (a: Mp-TiO_2; b: Sn(0.05)/Ti; c: Sn(0.10)/Ti; d: Sn (0.15)/Ti; e: Sn(0.20)/Ti).

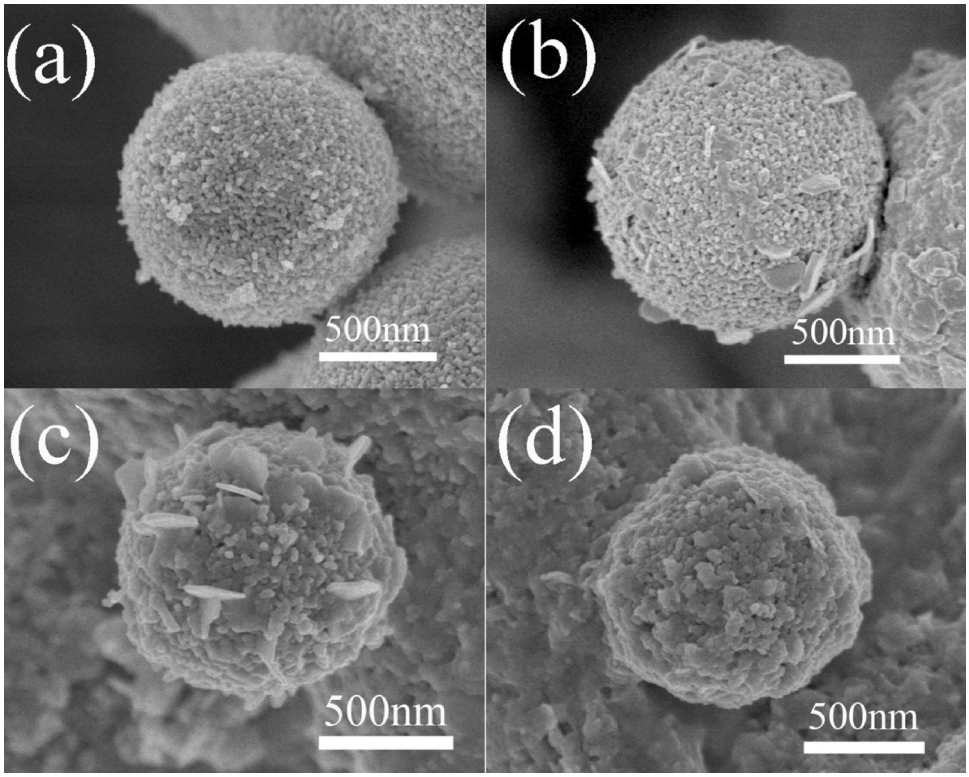

Fig. 2. SEM images of Mp-TiO_2 and Mp-TiO_2/SnS_2 (a: Mp-TiO_2; b: Sn(0.05)/Ti; c: Sn(0.10)/Ti; d: Sn(0.20)/Ti).

synthesis of SnS_2. Fig. S1 shows the Raman spectra of all the as-prepared samples. Raman spectra confirmed the presence of SnS_2 with a weak peak of 314.7 cm^{-1} [30]. The peaks at 150.8 cm^{-1}, 398.6 cm^{-1}, 517.2 cm^{-1}, and 639.7 cm^{-1} for catalysts were attributed to the *Eg*1, *B*1g, *B*1g + *A*1g, and *Eg*2 vibration modes of anatase TiO_2 symmetries [31,32].

The morphology of Mp-TiO_2 and Mp-TiO_2/SnS_2 were observed by scanning electron microscopy (SEM) (Fig. 2). As shown by the SEM image of pure MP-TiO_2 (Fig. 2a), the TiO_2 spheres with an average diameter of 1.1–1.3 μm comprise a great amount of TiO_2 nano-particles. Their unique homogeneous wormhole-like mesostructure [29] provides them with more active sites in photocatalytic reaction. After the hydrothermal process, the Mp-TiO_2 spheres were surrounded uniformly by SnS_2 (Fig. 2b–d and Fig.S2). When Sn/Ti molar ratios were 0.05 and 0.10, the SnS_2 nanosheets with a thickness of 10–20 nm (Fig.S3) were embedded in the Mp-TiO_2 spheres (Fig. 2b and c). With the molar ratio of Sn gradually increased, the as-prepared SnS_2 turned into nanoparticle and closely packed on the surface of Mp-TiO_2 (Fig.2d and Fig.S2) spheres. The change in the morphology of SnS_2 could be attributed to the different pH values of the synthesis system. With the increase of $SnCl_4{\cdot}5H_2O$ and TAA addition, the pH values of the solution decreased from 2.2, 1.9, 1.7 to 1.4, respectively. As reported previously, SnS_2 nanoparticles are more likely to form under strong acidic conditions [33]. Instead of growing on the surface of TiO_2 nanoparticles through heterogeneous nucleation, the high concentration of Sn^{4+} enabled the homogeneous nucleation of SnS_2 nanoparticles. Nanoparticles formed in the solution deposited on the surface of TiO_2 particles and formed Mp-TiO_2/SnS_2 particles with SnS_2 nanoparticles closely packed on the surface. The Schematic illustration of the preparation process of Mp-TiO_2/SnS_2 composites is shown in Scheme 1.

Nitrogen adsorption-desorption isotherms and the corresponding pore size distributions of the catalysts are shown in Fig. 3. The BET results indicated that the as-prepared anatase TiO_2 microspheres have a mesoporous structure with an average pore size of about 14.2 nm. Compared with pure Mp-TiO_2, the surface area of the compound

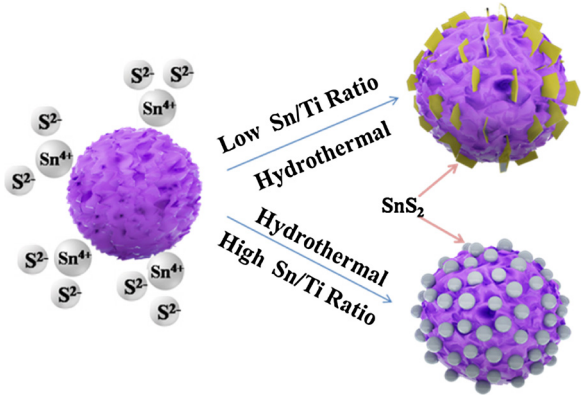

Scheme 1. Schematic illustration of the preparation process of Mp-TiO_2/SnS_2 composites.

materials increased after loading SnS_2. The pore volume and the pore size of Mp-TiO_2/SnS_2 decreased as the Sn/Ti molar ratio increased, which indicated the blocking of pores by the growth of SnS_2 nanoparticles (Table 1).

The absorption spectra of Mp-TiO_2 and as-prepared Mp-TiO_2/SnS_2 composite films in the wavelength range of 350–800 nm are shown in Fig. 4a. Compared with pure Mp-TiO_2, the combination with SnS_2 led to a visible red shift in the absorption edge of the hybrid material, which indicated that the coupling with SnS_2 could effectively increase the light harvesting ability of Mp-TiO_2 catalysts due to the smaller bandgap of SnS_2. In particular, Sn(0.10)/Ti exhibited the most obvious red shift among all the samples. In order to get a clear view of the changes in the light absorption properties of hybrid material with different Sn/Ti molar ratios, the indirect optical band gap (Eg) of Mp-TiO_2/SnS_2 composites was calculated according to the following equation [34–36]:

$$(\alpha h\nu)^2 = A(h\nu - Eg) \quad (1)$$

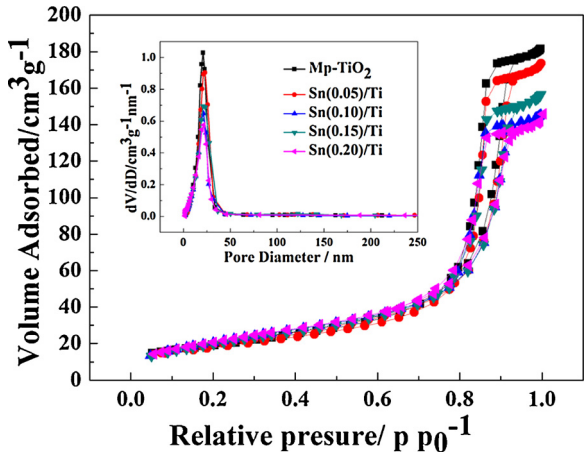

Fig. 3. Nitrogen adsorption-desorption isotherms and the corresponding pore size distribution curves.

Table 1
Physical properties of the photocatalysts.

Sample	S_{BET} ($m^2 g^{-1}$)	V_{pore} ($cm^3 g^{-1}$)	Pore size (nm)
Mp-TiO_2	71.3	0.31	14.3
Sn(0.05)/Ti	72.0	0.30	14.4
Sn(0.10)/Ti	78.4	0.24	13.3
Sn(0.15)/Ti	74.7	0.24	13.5
Sn(0.20)/Ti	79.0	0.22	11.7

Where h is the Planck constant, ν is the photon frequency, α is the absorption coefficient, Eg is the band gap and A is a constant. This means that a plot of $(\alpha h\nu)^2$ versus $h\nu$ should be a straight line with an intercept on the $h\nu$ axis equal to Eg.

Fig. 4b gives the plot of $(\alpha h\nu)^2$ vs. $h\nu$, which shows the indirect band gap values of as-prepared catalysts calculated based on Eq. (1). The Eg values of Mp-TiO_2, Sn(0.05)/Ti, Sn(0.10)/Ti, Sn(0.15)/Ti and Sn(0.20)/Ti were 3.11 eV, 2.67 eV, 2.24 eV, 2.45 eV and 2.35 eV, respectively (Table 2). The optimal light absorption performance for the effective utilization of visible light in the solar spectrum was obtained when Sn/Ti molar ratio reached 0.10 due to its small band gap. The high light-harvesting capability of Sn(0.10)/Ti would significantly improve its photocatalytic performance in the photodegradation of gaseous pollutants.

Photoluminescence spectra (PL) were used to observe the separation efficiency of the charge carriers of pure Mp-TiO_2 and Mp-TiO_2/SnS_2 compound catalysts. As shown in Fig. 5, the PL intensity of Mp-TiO_2/SnS_2 was much lower than that of pure Mp-TiO_2 in the wavelength range around 400 nm. This result manifested that the electron-hole

Table 2
Band-gap values of Mp-TiO_2 and Mp-TiO_2/SnS_2 composite films.

Sample	Mp-TiO_2	Sn(0.05)/Ti	Sn(0.10)/Ti	Sn(0.15)/Ti	Sn(0.20)/Ti
Bandgap/eV	3.10	2.67	2.24	2.45	2.35

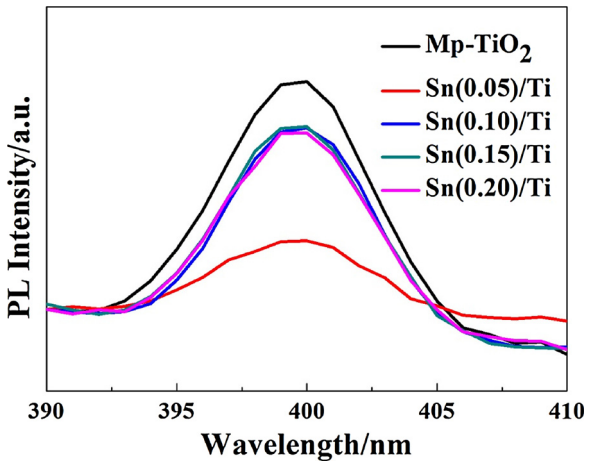

Fig. 5. Photoluminescence spectra (PL) of pure Mp-TiO_2 and Mp-TiO_2/SnS_2.

recombination was hindered by the formation of the heterostructure between TiO_2 and SnS_2 in Mp-TiO_2/SnS_2 compounds. Furthermore, Sn(0.05)/Ti had the minimum PL peak intensity in all samples, which illustrated that a small amount of SnS_2 modification can effectively promote the separation of electron and hole. With increasing SnS_2 loading, a portion of SnS_2 stacked together without direct contact with Mp-TiO_2, the separation of electron hole pairs would be restricted, which was inconsistent with the previous publication [37].

A smog chamber was used in this study to investigate the photocatalytic activity of the Mp-TiO_2/SnS_2 composite catalysts with a fluorescence light as the light source. HCHO injected into the smog chamber with the concentration of 2.5 ppm was used to simulate the indoor low concentration pollutants. Fig. 6 gives the photocatalytic decomposition curves of formaldehyde in the presence of Mp-TiO_2 or Mp-TiO_2/SnS_2 composite films under the illumination of a low power light (40 W). The C/C_0 curve of Mp-TiO_2 got increased from 0 min to 50 min. The most probable cause is that the photocatalytic performance of Mp-TiO_2 under the used 2*20 w fluorescent lamps was not good enough to decompose the adsorbed gas molecules in time. Some adsorbed HCHO molecules would evaporate to the gas bag due to the increased temperature caused by the heat of the fluorescent lamps, which led to this phenomenon. Compared with pure Mp-TiO_2, most Mp-TiO_2/SnS_2 compound catalysts showed great advantages in the

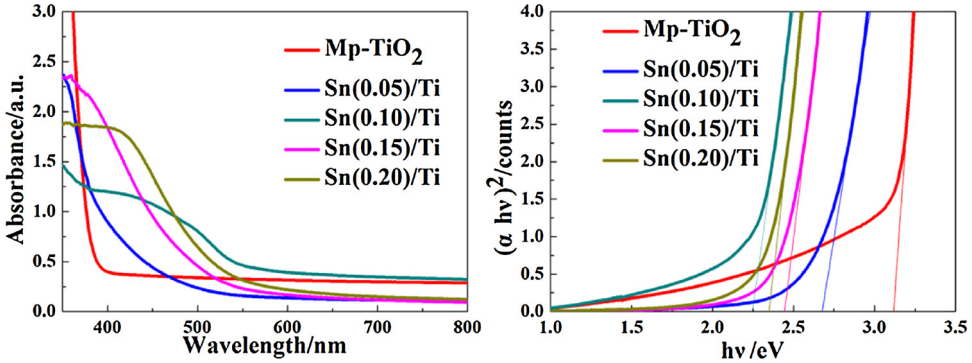

Fig. 4. (a): UV–vis absorption spectra of Mp-TiO_2 and as-prepared Mp-TiO_2/SnS_2 composite films with different Sn/Ti molar ratio; (b): band gap energy of Mp-TiO_2 and as-prepared Mp-TiO_2/SnS_2 composite films with different Sn/Ti molar ratio.

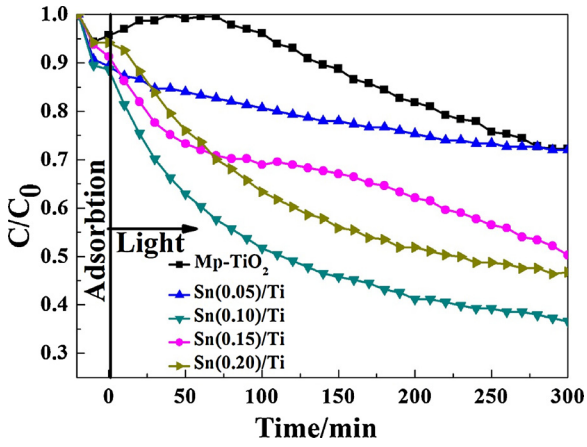

Fig. 6. Photocatalytic decomposition curves of HCHO in the presence of TiO_2/SnS_2 under indoor light.

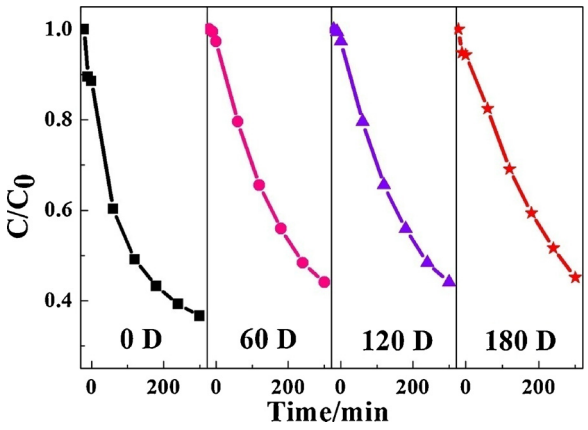

Fig. 7. Repeatability tests of Sn(0.10)/Ti.

degradation of HCHO, with more than 63% HCHO being removed in 300 min when the Sn/Ti molar ratio was 0.10. On the one hand, as shown in Fig. 2, for Mp-TiO_2/SnS_2 composite catalysts with a Sn/Ti molar ratio of 0.05, only a small amount of SnS_2 nanosheets was observed on the surface of Mp-TiO_2 nanospheres. Meanwhile, the redshift of the absorption edge of Sn(0.05)/Ti was almost neglectable in the UV–vis absorption spectra. Those results mean that if the content of SnS_2 is too low, only a small amount of electron-hole pairs can be generated under visible light irradiation. Therefore, although composite catalyst had the lowest recombination rate of electron-hole-hairs, the photocatalytic efficiency of Sn(0.05)/Ti remained low; in addition, when the precipitated amount of SnS_2 was increasing, the Mp-TiO_2 surface would be coated with a layer of dense nano-sized SnS_2 particles, which result in a decrease of pore volume and pore size of the compound catalysts. Therefore, surface activity sites decrease because of a fraction of SnS_2 growing in the pore of Mp-TiO_2. Meanwhile, excessive amounts of SnS_2 stacked together without direct contact with Mp-TiO_2, which restrained the separation of electron hole pairs. All these reasons may explain why the efficiency of Sn(0.10)/Ti was higher than in case of other catalysts. The band diagram of Mp-TiO_2/SnS_2 composite is shown in Scheme 2. According to the reported literature, the potential reaction processes are as follows [38]:

$$TiO_2/SnS_2 \xrightarrow{hv} e^- + h^+ \quad (2)$$

$$h^+ + H_2O \rightarrow \bullet OH + H^+ \quad (3)$$

$$e^- + O_2 \rightarrow \bullet O_2^- \quad (4)$$

$$HCHO + \bullet OH \rightarrow \bullet CHO + H_2O \quad (5)$$

$$\bullet CHO + \bullet OH \rightarrow HCOOH \quad (6)$$

$$\bullet CHO + \bullet O_2^- \rightarrow HCO_3^- \xrightarrow{H^+} HCOOOH \xrightarrow{HCHO} HCOOH \quad (7)$$

Table 3
Sn/Ti molar ratio of Sn(0.10)/Ti for the different storage period in the air.

Storage period	fresh sample	2 months	4 months	6 months
Sn/Ti	0.096	0.087	0.084	0.085

$$HCOOH \xrightarrow{-H^+} HCOO^- \xrightarrow{h^+} H^+ + \bullet CO_2^- \quad (8)$$

$$\bullet CO_2^- \xrightarrow{[O],\bullet OH,h^+} CO_2 \quad (9)$$

The outstanding photocatalytic performance of Mp-TiO_2/SnS_2 composite photocatalysts under low power indoors light could be attributed to the enhanced light harvesting efficiency caused by the multiple reflection of incident light between Mp-TiO_2 and the effective separation of electron-hole pairs due to the formation of heterojunction structures As reported previously [39], the multiple light reflections existed between cambered surfaces of 'yolk' and 'shell'. In the 'yolk-shell' structure TiO_2 could effectively enhance its light harvesting capacity. Similar to the 'yolk-shell' structure, the heterojunction structure formed by SnS_2 nanosheets and Mp-TiO_2 spheres in our work could also improve the light utilization efficiency of hybrid photocatalysts through extending the light path (Scheme 2). When light reached the surface of Mp-TiO_2 spheres, attenuation would happen due to the absorption of light by SnS_2. The unabsorbed light would then be reflected by TiO_2 spheres and resorbed by SnS_2, which enabled the full utilization of the incident light and the high light-harvesting efficiency of composite photocatalysts. Besides, the combination with SnS_2 could also promote the separation of electron and hole due to the differences in the band structures of TiO_2 and SnS_2 [40]. Compared to the reported works [25,41–43], the light harvesting efficiency of the composite materials was enhanced due to the diffuse reflection of incident light on the rough surface of Mp-TiO_2 effectively. In addition, mesoporous TiO_2 spheres had a unique homogeneous wormhole-like mesostructure, which was

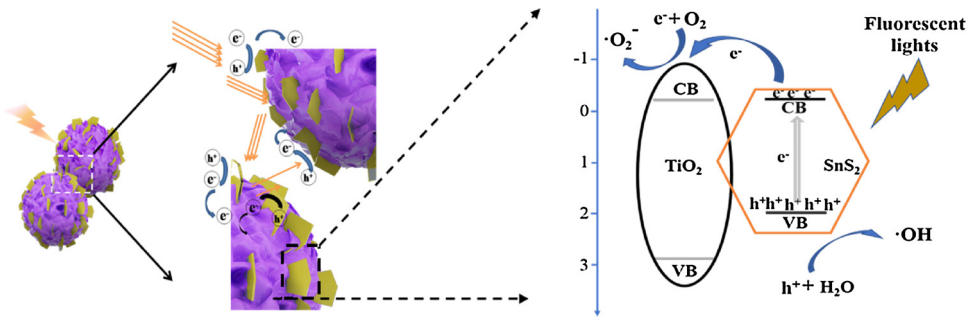

Scheme 2. The multiple light reflections mechanism and the band diagram of Mp-TiO_2/SnS_2 composite.

considered to provide more active sites in the photocatalytic process. Meanwhile, the degradation efficiency of Sn(0.10)/Ti had been proved to decrease only 10% in a long-term study for half a year, which can support the long-term applications of Mp-TiO_2/SnS_2 composite. The result that Mp-TiO_2/SnS_2 compound photocatalyst shows outstanding performance under low power indoors light, would greatly promote the practical application of TiO_2-based photocatalytic materials for the indoor air purification.

The chemical stability of the photocatalysts is very important for practical applications. In the purpose of evaluating the stability of Sn (0.10)/Ti in the photocatalytic decomposition of HCHO, the photocatalytic performance of Sn(0.10)/Ti was measured repeatedly after being exposed to the air for 2, 4 and 6 months. At the end of each test, the catalyst was rinsed with ionized water and dried at room temperature. As shown in Fig. 7, the photodegradation efficiency of Sn (0.10)/Ti decreased by about 10% in the first 2 months. Interestingly, the efficiency remained stable at about 55% in the following four months. In the purpose of understanding the changes in the photocatalytic performance of Mp-TiO_2/SnS_2 composite photocatalysts, the quantitative changes of Sn, Ti elements of Sn(0.10)/Ti sample during the aging period were determined by Energy-Dispersive Spectrometer (EDS). As shown in Table 3 (the EDS images are shown in Fig.S4), the Sn/Ti molar ratio of the fresh Sn(0.10)/Ti was 0.096, which is very close to the theoretical value. After being aged for 2 months, this ratio went down from 0.096 to 0.087. Interestingly, the Sn/Ti molar ratio remained relatively stable for longer storage time. Hence, the lack of SnS_2 was considered as the main reason for the attenuation of the catalytic performance in the first 2 months. Meanwhile, it also confirmed the excellent stability of Sn(0.10)/Ti in the long-term practical applications.

4. Conclusion

Herein, Mp-TiO_2/SnS_2 composite photocatalysts were synthesized through an in-situ hydrothermal process. By controlling the concentration of $SnCl_4$ in the reaction system, SnS_2 nanometer materials could be uniformly deposited onto the surface of Mp-TiO_2 spheres. MP-TiO_2/SnS_2 composite spheres with a rough surface and a heterojunction structure could be achieved. The modification of Mp-TiO_2 with SnS_2 nanosheets could not only broaden the light absorption range of the photocatalysts, but also enabled the effective separation of photo-induced electron-hole pairs, which significantly improved the performance of composite photocatalysts. Due to the increase of light harvesting capacity and the decrease of the recombination rate of photogenerated electron hole pairs, the as-prepared Mp-TiO_2/SnS_2 nanocomposites exhibited excellent photocatalytic activity in the decomposition of HCHO under low power indoor light irradiation. This is meaningful for the practical application of TiO_2-based photocatalysts in the indoor air purification field. An optimal degradation efficiency was achieved when the molar ratio of SnS_2/TiO_2 was 0.10. In addition, Mp-TiO_2/SnS_2 exhibited excellent long-term chemical stability in the air, which is very beneficial to the long-term applications of photocatalysts.

Conflicts of interest

There are no conflicts to declare.

Acknowledgements

This work was financially supported by the National Key Research and Development Program of China (2016YFA0203000), the International Partnership Program of Chinese Academy of Sciences (GJHZ1656) and the NSFC-DFG bilateral organization program (51761135107 and SE 2526-3/1).

Appendix A. Supplementary data

Supplementary material related to this article can be found, in the online version, at doi:https://doi.org/10.1016/j.jphotochem.2018.06.043.

References

[1] B. Bai, J. Li, Positive effects of K^+ ions on three-dimensional mesoporous Ag/Co_3O_4 catalyst for HCHO oxidation, ACS Catal. 4 (8) (2014) 2753–2762.
[2] H.Y. Chen, et al., ZnO modified TiO_2 nanotube array supported Pt catalyst for HCHO removal under mild conditions, Catal. Today 264 (2016) 23–30.
[3] Y. Le, et al., Bio-template-assisted synthesis of hierarchically hollow SiO_2 microtubes and their enhanced formaldehyde adsorption performance, Appl. Surf. Sci. 274 (2013) 110–116.
[4] F. Shiraishi, S. Ikeda, N. Kamikariya, Photocatalytic decompositions of gaseous HCHO over thin films of anatase titanium oxide converted from amorphous in a heated air and in an aqueous solution of hydrogen peroxide, Chem. Eng. J. 148 (2–3) (2009) 234–241.
[5] Z.H. Xu, J.G. Yu, M. Jaroniec, Efficient catalytic removal of formaldehyde at room temperature using AlOOH nanoflakes with deposited Pt, Appl. Catal. B-Environ. 163 (2015) 306–312.
[6] L.F. Qi, et al., Enhanced catalytic activity of hierarchically macro-/mesoporous Pt/TiO_2 toward room-temperature decomposition of formaldehyde, Catal. Sci. Technol. 5 (4) (2015) 2366–2377.
[7] A.Y. Chen, et al., Effect of annealing atmosphere on the thermal coarsening of nanoporous gold films, Appl. Surf. Sci 355 (2015) 133–138.
[8] H. Chen, et al., ZnO modified TiO_2 nanotube array supported Pt catalyst for HCHO removal under mild conditions, Catal. Today 264 (2016) 23–30.
[9] Y. Li, et al., High temperature reduction dramatically promotes Pd/TiO_2 catalyst for ambient formaldehyde oxidation, Appl. Catal. B-Environ. 217 (2017) 560–569.
[10] Y. Bai, et al., Template method to controllable synthesis 3D porous $NiCo_2O_4$ with enhanced capacitance and stability for supercapacitors, J. Colloid Interface Sci. 468 (2016) 1–9.
[11] B.P. Bastakoti, N.L. Torad, Y. Yamauchi, Polymeric micelle assembly for the direct synthesis of platinum-decorated mesoporous TiO_2 toward highly selective sensing of acetaldehyde, ACS Appl. Mater. Interfaces 6 (2) (2014) 854–860.
[12] Z.N. Han, et al., Experimental study on visible-light induced photocatalytic oxidation of gaseous formaldehyde by polyester fiber supported photocatalysts, Chem. Eng. J. 218 (2013) 9–18.
[13] D. Maruthamani, D. Divakar, M. Kumaravel, Enhanced photocatalytic activity of TiO_2 by reduced graphene oxide in mineralization of Rhodamine B dye, J. Ind. Eng. Chem. 30 (2015) 33–43.
[14] A.Y. Chen, et al., Microstructure and electrocatalytic performance of nanoporous gold foils decorated by TiO_2 coatings, Surf. Coat. Tech. 286 (2016) 113–118.
[15] G. Cheng, et al., A novel protocol to design TiO_2-Fe_2O_3 hybrids with effective charge separation efficiency for improved photocatalysis, Adv. Powder Technol. 28 (2) (2017) 665–670.
[16] C.C. Wang, et al., Deposition of uniform Pt nanoparticles with controllable size on TiO_2-based nanowires by atomic layer deposition and their photocatalytic properties, Nanotechnology 26 (25) (2015) 254002.
[17] C. Chen, W. Ma, J. Zhao, Semiconductor-mediated photodegradation of pollutants under visible-light irradiation, Chem. Soc. Rev 39 (11) (2010) 4206–4219.
[18] M.V. Dozzi, E. Selli, Doping TiO_2 with p-block elements: Effects on photocatalytic activity, J. Photochem. Photobiol. C 14 (2013) 13–28.
[19] S. Pany, K.M. Parida, A facile in situ approach to fabricate N,S-TiO_2/g-C_3N_4 nanocomposite with excellent activity for visible light induced water splitting for hydrogen evolution, Phys. Chem. Chem. Phys. 17 (12) (2015) 8070–8077.
[20] S. Li-Xia, Z. Yang-Bo, TiO_2 nanoring/nanotube hierarchical structure growth mechanism and optical absorption property, J. Inorg. Mater. 32 (12) (2017) 1327.
[21] M. Khatamian, et al., Visible-light response photocatalytic water splitting over CdS/TiO_2 and CdS-TiO_2/metalosilicate composites, Int. J. Energy Res. 38 (13) (2014) 1712–1726.
[22] C.C. Chan, et al., Efficient and stable photocatalytic hydrogen production from water splitting over $Zn_xCd_{1-x}S$ solid solutions under visible light irradiation, Int. J. Hydrogen Energy 39 (4) (2014) 1630–1639.
[23] K. Ullah, et al., Synthesis and characterization of novel PbS–graphene/TiO_2 composite with enhanced photocatalytic activity, J. Ind. Eng. Chem. 20 (3) (2014) 1035–1042.
[24] Z. Zhang, et al., Hierarchical assembly of ultrathin hexagonal SnS2 nanosheets onto electrospun TiO_2 nanofibers: enhanced photocatalytic activity based on photo-induced interfacial charge transfer, Nanoscale 5 (2) (2013) 606–618.
[25] K.C. Christoforidis, et al., Single-step synthesis of SnS_2 nanosheet-decorated TiO_2 anatase nanofibers as efficient photocatalysts for the degradation of gas-phase diethylsulfide, ACS Appl. Mater. Interfaces 7 (34) (2015) 19324–19334.
[26] M.M. Gao, et al., Structural design of TiO2-based photocatalyst for H_2 production and degradation applications, Catal. Sci. Technol. 5 (10) (2015) 4703–4726.
[27] C.-P. Hsu, et al., EIS analysis on low temperature fabrication of TiO_2 porous films for dye-sensitized solar cells, Electrochim. Acta 53 (25) (2008) 7514–7522.
[28] Q. Zhang, et al., Three-dimensional TiO_2 nanotube arrays combined with g-C_3N_4 quantum dots for visible light-driven photocatalytic hydrogen production, RSC Adv. 7 (22) (2017) 13223–13227.
[29] D. Chen, et al., Synthesis of monodisperse mesoporous titania beads with

controllable diameter, high surface areas, and variable pore diameters (14-23 nm), J. Am. Chem. Soc. 132 (12) (2010) 4438–4444.
[30] X. Zhang, et al., Template-oriented synthesis of monodispersed SnS_2@SnO_2 heterostructured nanoflowers for Cr(VI) photoreduction, Appl. Catal. B-Environ. 192 (2016) 17–25.
[31] D.N. Joshi, et al., Swift sol–gel synthesis of mesoporous anatase-rich TiO_2 aggregates via microwave and a lyophilization approach for improved light scattering in DSSCs, J. Mate. Sci. 52 (4) (2016) 2308–2318.
[32] J. Zhang, et al., UV Raman spectroscopic study on TiO_2. I. Phase transformation at the surface and in the bulk, J. Phys. Chem. B 110 (2) (2006) 927–935.
[33] X.L. Gou, J. Chen, P.W. Shen, Synthesis, characterization and application of SnS_x (x=1, 2) nanoparticles, Mater. Chem. Phys. 93 (2-3) (2005) 557–566.
[34] H.Y. He, J. Fei, J. Lu, Optical and electrical properties of pure and Sn^{4+} doped n-SnS films deposited by chemical bath deposition, Mat. Sci. Semicom. Proc. 24 (2014) 90–95.
[35] O.E. Ogah, et al., Thin films of tin sulphide for use in thin film solar cell devices, Thin Solid Films 517 (7) (2009) 2485–2488.
[36] S. Sohila, et al., Optical and Raman scattering studies on SnS nanoparticles, J. Alloy Compd. 509 (19) (2011) 5843–5847.
[37] J. Li, T. Wang, X. Du, Preparation of visible light-driven SnS_2/TiO_2 nanocomposite photocatalyst for the reduction of aqueous Cr(VI), Sep. Purif. Technol. 101 (2012) 11–17.
[38] J.J. Yang, et al., A study of the photocatalytic oxidation of formaldehyde on Pt/Fe_2O_3/TiO_2, J. Photochem. Photobiol. A 137 (2000) 197–202.
[39] J. Wang, et al., Mesoporous yolk-shell SnS_2-TiO_2 visible photocatalysts with enhanced activity and durability in Cr(VI) reduction, Nanoscale 5 (5) (2013) 1876–1881.
[40] Z.Y. Wang, et al., Fabrication of $Bi_2O_2CO_3$/g-C_3N_4 heterojunctions for efficiently photocatalytic NO in air removal: in-situ self-sacrificial synthesis, characterizations and mechanistic study, Appl. Catal. B-Environ. 199 (2016) 123–133.
[41] J. Zhang, et al., Anatase TiO_2 nanosheets with coexposed {101} and {001} facets coupled with ultrathin SnS_2 nanosheets as a face-to-face n-p-n dual heterojunction photocatalyst for enhancing photocatalytic activity, Appl. Surf. Sci. 420 (2017) 839–848.
[42] F.F. Yang, et al., Improved photodegradation activity of TiO_2 via decoration with SnS_2 nanoparticles, Mater. Chem. Phys. 140 (1) (2013) 398–404.
[43] L. Deng, et al., SnS_2/TiO_2 nanocomposites with enhanced visible light-driven photo reduction of aqueous Cr(VI), Ceram. Int. 42 (3) (2016) 3808–3815.